Modelling of DEMO Core Plasma Consistent with SOL/Divertor Simulations for Long Pulse Scenarios

G.W. Pacher[1], H.D. Pacher[2], G. Janeschitz[3], A.S. Kukushkin[4], V. Kotov[5], D. Reiter[5]

1) Hydro-Québec, Varennes, Québec, Canada
2) INRS-EMT, Varennes, Québec, Canada
3) FZK-PL-Fusion, Karlsruhe, Germany
4) ITER IT, Garching, Germany
5) FZ Jülich, Jülich, Germany

e-mail contact of the main author: pacher.guenther@ireq.ca

Abstract. The Integrated Core-Pedestal-SOL model is applied to the simulation of typical DEMO operation. Impurity seeding is used to reduce the power load on the divertor to acceptable levels. The influence on long pulse operation of impurity seeding with various impurities is investigated.

1. Introduction

DEMO operation with self-consistent parameters for the core and edge is investigated using the Integrated Core Pedestal SOL Model (ICPS Model [1, 2]) in the 1.5D Astra code. The plasma core is coupled to the plasma edge via scaling relations obtained from B2-EIRENE simulations of the SOL and divertor [3]. Impurity seeding is applied in order to increase radiation from the plasma core and thereby lower the power load on the divertor. For a typical DEMO geometry (R = 8.1 m, a = 2.8 m, I ≤ 21 MA, B = 5.7 T), four different seed impurities are investigated, with particular emphasis on the implications of such impurity seeding on longer pulse operation.

2. Transport Model

The core energy transport is given by the MMM95 transport model [5, 6], stabilised by a combination of ExB velocity shear and magnetic shear as described in [1, 2], and is summarized as follows:

$$\chi = \chi_{MMM} \Big/ \left\{ \left(1+(\omega_{E\times B}/(G\,\gamma_0))^2\right) \cdot \max\left(1,(s-t)^2\right) \right\}$$

$$\omega_{E\times B} = \frac{RB_\theta}{B}\,\frac{\partial}{\partial r}\left(\frac{E}{RB_\theta}\right) \quad \text{and} \quad E = \nabla p_i/(n_i\,e)$$

(where γ_0, the volume average of γ_{ITG} inside 0.9 of the minor radius, is an estimate for the growth rate in the absence of stabilisation; $\omega_{E\times B}$ is the $E\times B$ shearing rate with R the major radius; and χ_{MMM} is the transport coefficient in the absence of shear). The first factor in curly brackets represents the $E\times B$ velocity shear stabilisation, and the second is the additional shear stabilisation, i.e. transport is reduced only in the region where shear s exceeds the threshold t and is unaffected elsewhere. For all simulations presented here, G=0.5 and t=0.5, a combination which has been shown [1,2] to reproduce well experimental results in JET and Asdex-UG. ELM's are treated in a time-average fashion by strongly increasing transport when the ballooning limit is exceeded, so that the pressure gradient is limited to that given by ballooning stability. The time-averaged pedestal height and width are thus determined self-consistently with ballooning stability.

Particle transport is determined according to:

$$D = D_{neo} + D_{an};\ \mathrm{v} = \mathrm{v}_{neo} + \mathrm{v}_{an} \quad \text{with } D_{an} = C_n(\chi_e + \chi_i) \text{ and } \mathrm{v}_{an} = C_\mathrm{v} D_n (2r/a^2)$$

The anomalous particle transport coefficient is thus proportional to the anomalous energy transport. C_n and C_v are equal for all species. As shown previously [2, section 2], the choice of $C_n = 0.1$, $C_v = 0$ reproduces well the density profiles in present experiments. The JET profile can also be produced with $C_n = 0.5$ and $C_v = 0.5$. However, only the first parameter combination will be used here. The effect of varying the particle transport on required impurity seeding and operating conditions has been considered in [7]. For helium, the diffusion coefficient and convective velocity are taken equal to those used for the hydrogen isotopes.

Inside the $q = 1$ surface, when it exists, the current profile is flattened by increasing the resistivity such that $q \sim 1$, and the transport coefficients are increased by a factor of four. Temperature and particle profiles are therefore also flattened inside the $q = 1$ surface, but less than the current profile.

In addition to the helium produced by the fusion reactions; two impurity species are considered in the simulations. The first is an intrinsic low-Z impurity which, in the present B2-Eirene modelling, is carbon. Even though carbon is unlikely to be used in DEMO, carbon is retained for now in core modelling to retain the effect of low-Z contamination of the plasma but with an edge density half of that resulting from the SOL modelling. The model contains an additional seeded medium- to high-Z impurity, which is not yet included in the SOL simulations. The edge density of this seed impurity, employed to reduce the divertor power load, is therefore an independent input parameter for now.

For impurities other than helium, theoretical neoclassical transport coefficients are used, as determined according to the routine NCLASS [8]. This results in flat or slightly hollow profiles for impurity species other than helium [7]. For DEMO as for ITER, direct fuelling inside the pedestal is required to sustain the operating density because the SOL is almost opaque to neutrals injected into the vacuum vessel and therefore the neutral DT flux across the separatrix is insufficient to fuel the plasma. Core fuelling is provided by a particle source profile peaked just inside the separatrix with a full-width at half-maximum (FWHM) of 29 cm.

3. SOL-Divertor Simulations and the Edge-Based Density Limit

The scaling of the principal edge plasma parameters for ITER has been established from extensive SOL-Divertor simulations with B2-EIRENE in [3]. The key parameter for characterising the edge plasma operational point is μ, the neutral pressure normalized to 1 at detachment of the inner divertor. Simulations for DEMO have resulted in an extension of these scalings [4]. The results are found to agree well with powers of $R_\#$, the ratio of the outer strike point radii for DEMO and ITER. They are now expressed in terms of $P_\#$, the power normalised by $R_\#^3$, and $S_\#$, the pumping speed normalised by $R_\#^2$, with additional size factors in terms of $R_\#$. Other factors for type of fuelling, wall, neutral model, and connection length are given in [3, 4]. The normalized neutral pressure is found to be, for DEMO [4]: $\mu \equiv p_{DT\#} P_\#^{-0.87} f_f^{-0.8} f_w^{-1} q_{95\#}^{-0.27} f_{nn}^{-1} R_\#^{-1.21}$. Here $p_{DT\#}$ is the average divertor neutral pressure at the entrance to the private flux region.

The edge-based density limit occurs at detachment of the inner divertor ($\mu = 1$). Simulations with the linear neutral model and intrinsic carbon impurity (carbon-covered walls) show [4] that the key parameters scale favourably from ITER to DEMO. In fact, at the same SOL

power per unit volume of the device, and the same specific pumping speed for ITER and DEMO, the separatrix helium density remains constant ($\sim R_{\#}^{0.15}$), the helium neutral influx decreases ($\sim R_{\#}^{-1.46}$), and the peak power loading of the divertor plates remains constant ($\sim R_{\#}^{-0.02}$) in the transition from ITER to DEMO.
These scalings [4] are then used for the coupled DEMO simulations. (Further improvement in helium found in initial modelling runs with the more complete full neutral model [4] is not yet implemented in the full modelling.)

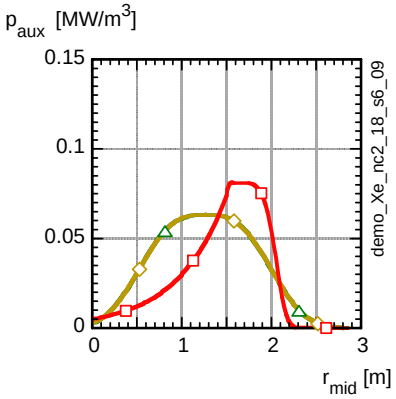

Fig. 1 - Additional power density profiles: green & beige - "profile 0.4a", red - "profile 0.7a"

4. Description of the simulations

Because of the large disparity of characteristic time scales of the core plasma and the SOL/divertor region, it is impracticable to cover both regions in a single simulation. Instead, they are linked at the separatrix, with outer boundary conditions for the core obtained from SOL/divertor runs, and inner boundary conditions for SOL/divertor parameters resulting from simulation of the core. The core-pedestal (1.5D code ASTRA), and the SOL-divertor (2D code B2-Eirene) regions are thus linked via scaling relations [4] and consistency of operating conditions in both regions is assured. Inputs to ASTRA include separatrix DT, He, and C densities, separatrix ion and electron temperatures, and separatrix inward neutral DT and He fluxes. Outputs from ASTRA (inputs to the scaling relation) are the power transported across the separatrix by electrons, that transported by ions, the fusion power, and the DT flux into the SOL. (The He ion flux is the sum of production by fusion and neutral influx). The control parameters for the core simulation are the core fuelling flux Γ_{core}, the gas puff flux into the vessel Γ_{puff}, and the additional heating power P_{aux}. An additional control parameter is the edge density of the seed impurity $n_{Z,edge}$.

For each of four seed impurities (Ne, Ar, Fe, and Xe), a quasi-time-dependent simulation of the core/pedestal is carried out, in which the plasma is allowed to relax as the edge impurity density $n_{Z,edge}$ is increased in a step-wise fashion. The core fuelling flux Γ_{core} is controlled to obtain the desired fusion power of ~3 GW. The gas puff rate Γ_{puff} is adjusted for a given operating point, i.e. a given fraction μ of the edge-based density limit defined above. All simulations presented here are at $\mu = 0.7$, i.e. 70% of the edge-based density limit. The maximum divertor power load q_{pk} from the scaling relation is an output of the simulation.

In order to investigate long-pulse operation, conditions at a plasma current of 18 MA were compared with those at nominal 21 MA operation. Additional heating and current drive power P_{aux} was fixed at 50 MW, giving Q = 60, i.e. the plasma is essentially ignited. The current driven by the additional heating power is taken proportional to the heating power density and inversely proportional to the local plasma density, i.e.

$$j_{CD}[MA\ m^{-2}] = K_{CD}[MA\ MW^{-1}m^{-2}] \cdot p_{aux}[MW\ m^{-3}] / n_e[10^{20}\ m^{-3}]$$

The proportionality factor K_{CD} is held fixed for most of the simulations (it is set to zero to compare the effect of heating power alone with that obtained from combined heating and current drive). Near-axis (maximum near mid-radius with a wide and symmetrical profile - "profile *0.4a*") and off-axis (maximum near 70% of minor radius with asymmetric profile - "profile *0.7a*") power deposition is investigated with a view to optimising the long pulse capability. These deposition profiles are shown in figure 1.

The total plasma current is held fixed at the desired value as the seed impurity concentration is varied, so that the loop voltage necessary to maintain this current, in the presence of the current driven by P_{aux} and the neoclassical bootstrap current as determined from NCLASS [8] is thus the figure of merit for long-pulse operation.

5. Results

Figure 2 shows the profiles obtained for the case of Xenon seeding sufficient to lower the peak divertor load q_{pk} to a value near 5 MW/m^2. At a plasma current of 21 MA in the absence of current drive (K_{CD} = 0) with heating profile *"0.4a"*, the temperature is flattened inside 0.25 *a* (the mid-plane minor half-axis), leading to a suppression of bootstrap current near the centre. With the same additional power profile, but with current drive activated (K_{CD} = 5), the q = 1 region shrinks, thereby allowing a higher central temperature. Consequently, the central bootstrap current increases. Off-axis current drive (profile *"0.7a"*) amplifies this effect somewhat (the effect is more pronounced at 18 MA - lower part of fig. 2). As a result, the loop voltage drops from ~30 mV through 16 mV to 12 mV for off-axis current drive.

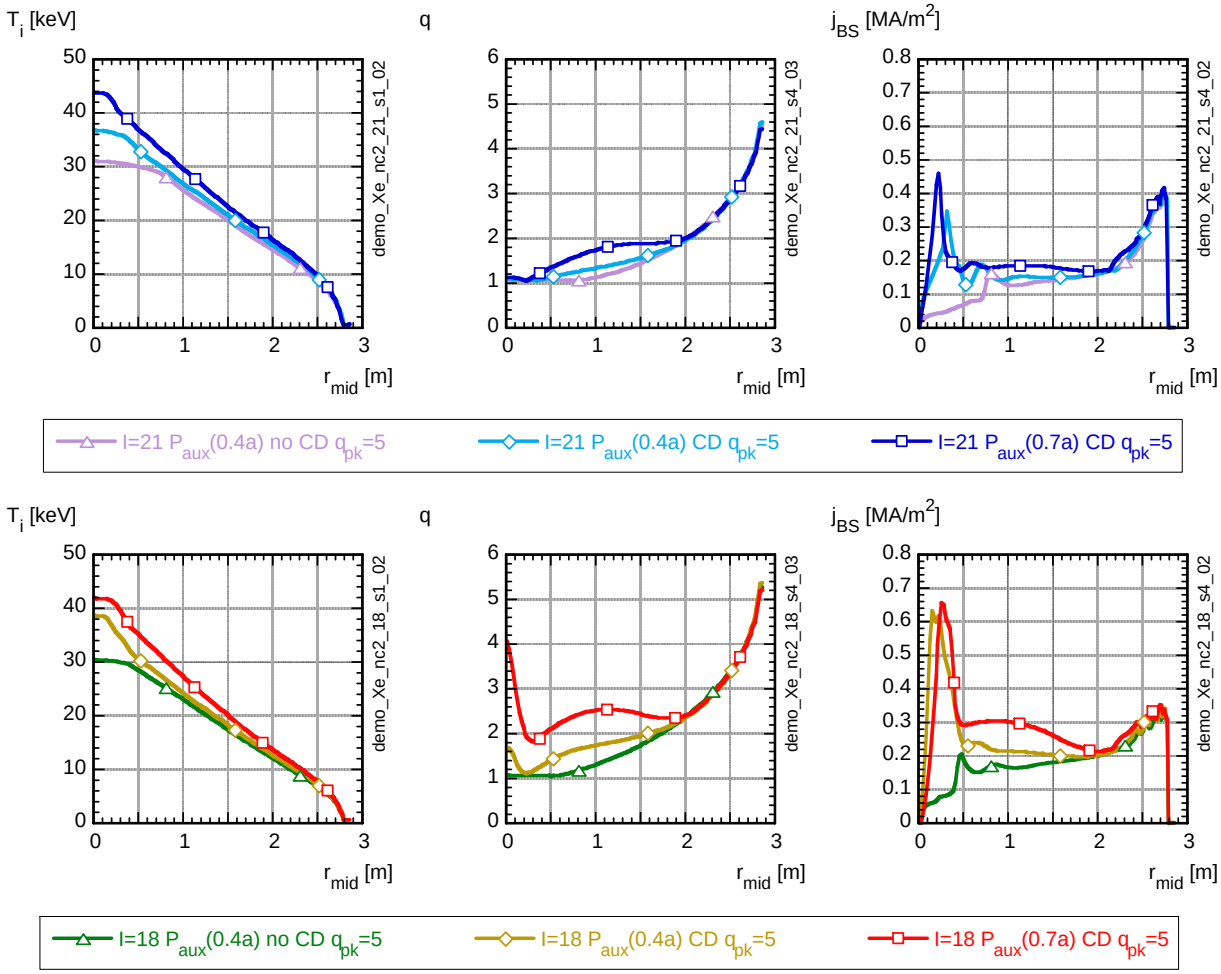

Fig. 2 - Radial profiles of T_i, q, and j_{BS} at 21 MA (top) and 18 MA (bottom) at q_{pk}~ 5 MW/m^2: violet & green -heating alone (profile 0.4a), light blue & beige -with current drive (profile 0.4a), dark blue & red - with current drive (profile 0.7a)

If the plasma current is lowered to 18 MA (bottom part of Fig. 2) a similar sequence is obtained. The loop voltage in the absence of current drive becomes ~23 mV, because the difference between total current and bootstrap current decreases, due to the reduction of plasma current and also to the increase of bootstrap current as compared with the 21 MA case.

As current drive is added, the resulting loop voltage decreases to 15 mV for profile *"0.4a"* and to 3 mV for off-axis current drive (profile *"0.7a"*). A separate comparison (not shown here) of the auxiliary power profile *"0.7a"*, without (K_{CD} = 0) and with (K_{CD} = 5) current drive led to the conclusion that the major effect results from the change of the bootstrap current profile brought about by the driven current. In particular, the loop voltage with off-axis heating alone is only 10% lower than that obtained for more central heating.

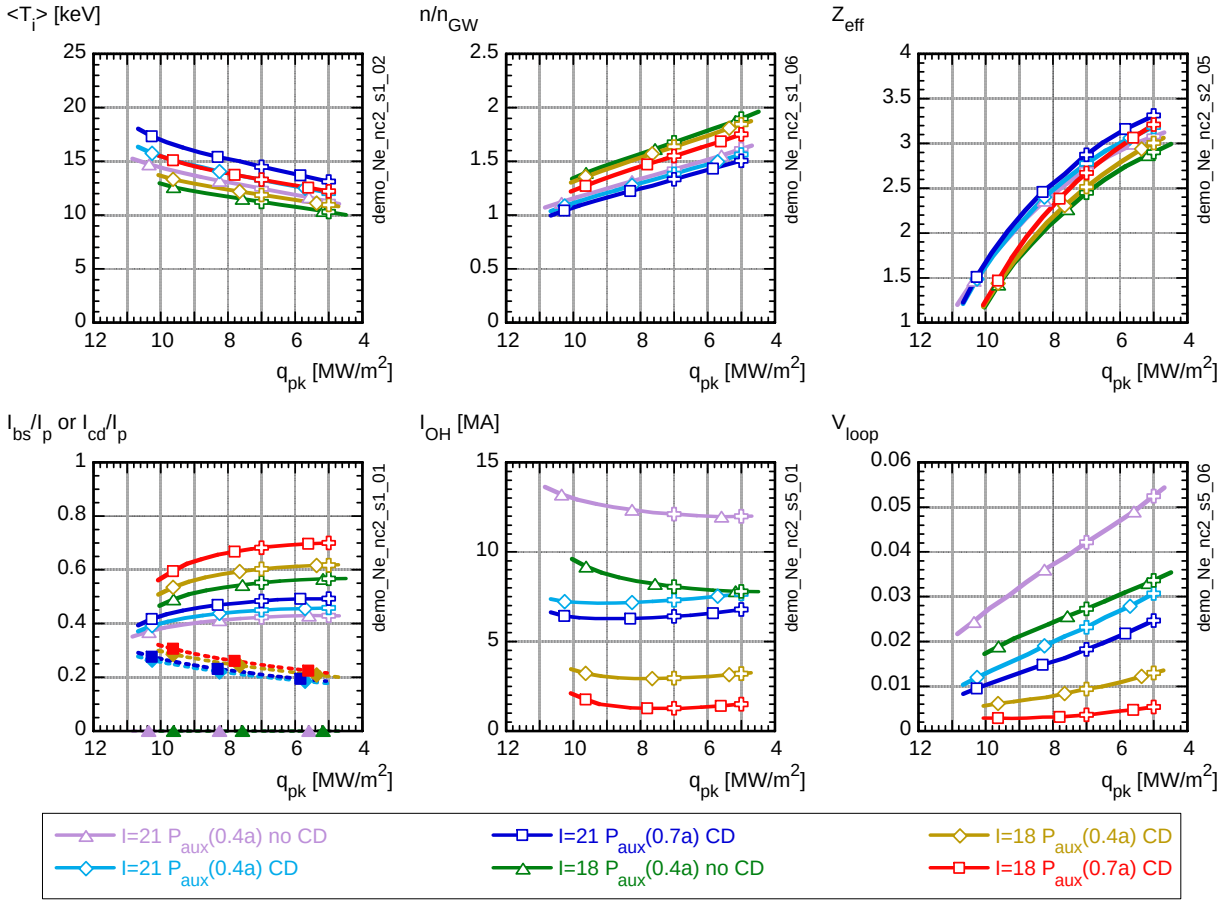

Fig. 3 - Parameter variation as Neon seeding is varied, plotted against peak divertor power load q_{pk}. Crosses indicate power load of 7 and 5 MW/m^2. Bottom left-hand figure shows fraction of current resulting from bootstrap (solid lines) and driven current (dashed lines)

Figures 3 and 4 show the variation of relevant parameters as the peak power load is decreased by seeding with the lowest- (Neon) and highest-Z (Xenon) impurity investigated at 21 and 18 MA for the various current drive scenarios. Lower current operation results in lower average ion temperatures and therefore requires higher densities for both impurities, tendencies which increase as impurity seeding is increased and the peak power load falls. However, the effect is amplified for the lower Z impurity because of increased dilution and therefore much higher Z_{eff} results. The higher dilution also requires higher beta to obtain the same fusion power, accompanied by a higher bootstrap current. For Neon seeding, the loop voltage increases by a factor of 2.5 for most conditions as the peak power load is lowered from 10 to 5 MW/m^2. The corresponding increase for Xenon seeding is only a factor of 1.5, i.e. for a given available flat-top flux, the pulse length is 60% longer for the high Z impurity than for the low Z impurity at the same power load.

Figure 5 summarizes the results for the four different impurities as plots in order of increasing atomic number at a peak divertor power load of 5 MW/m^2. As expected, all variations with increases of seeding (reduction of peak power load) vary similarly with the Z of the seed

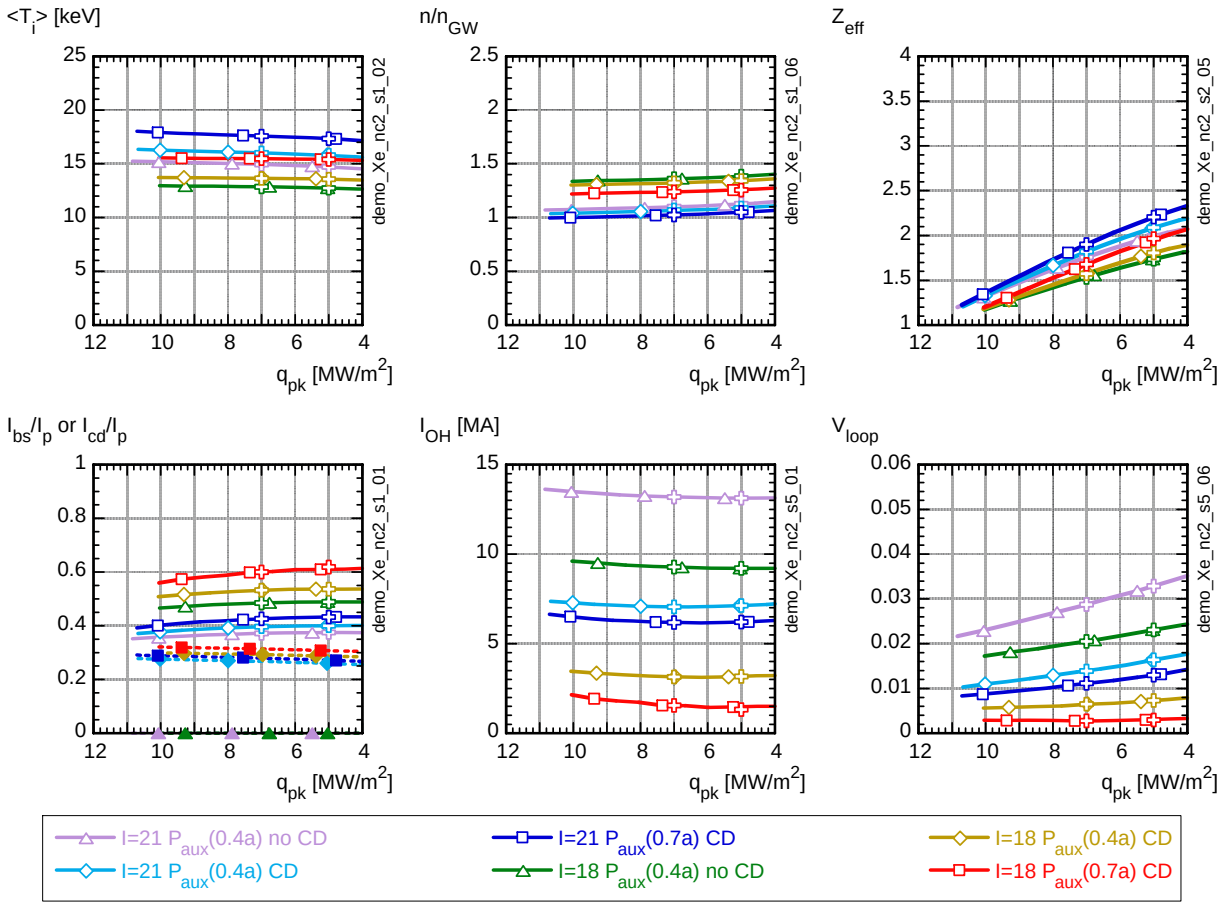

Fig. 4 - Parameter variation as Xenon seeding is varied, plotted against peak divertor power load q_{pk}. Crosses indicate power load of 7 and 5 MW/m^2. Bottom left-hand figure shows fraction of current resulting from bootstrap (solid lines) and driven current (dashed lines)

impurity.

As Z increases, the temperatures increase, the electron and DT densities decrease, the required core fuelling decreases, the bootstrap fraction decreases, and the driven current fraction increases. Because of the opposing effect of the two non-inductive current variations, the remaining inductive current (I_{OH}) has no strong variation with the Z of the seed impurity (if anything, it decreases with decreasing Z). Nevertheless, the required loop voltage decreases with increasing Z (note the log scale) because of the strong decrease of Z_{eff} as Z increases ($V_{loop} \propto Z_{eff}\, I_{OH}$). The tendencies are the same at 21 MA (left part of each plot) as at 18 MA (right part of each plot). Major differences as a function of current are the normalized beta β_N (not shown, for Xe: ≤2.8 at 21 MA, ≤3.1 at 21 MA; little variation with Z: ~0.1 higher for Ne) and n/n_{GW}, which are higher at lower plasma current, as well as I_{OH} and V_{loop}, which are lower. Long pulse operation is therefore favoured by lower plasma current, higher Z of the seed impurity, and flattened q profiles obtained with far off-axis current drive (profile *"0.7a"*), as shown on the bottom right-hand plot (100 Vs are assumed to be available for burn at 21 MA; this increases to ~150 Vs when the current is reduced to 18 MA).

With the parameter K_{CD} chosen here, the current drive efficiency deduced of $\eta = 0.7$ [10^{20} $MA\ m^{-2}\ MW^{-1}$] ($\eta \equiv I_{CD} \langle n_e \rangle R / P_{aux}$) is high, in excess of the value of 0.5 normally assumed to be a maximum. It has been verified that with an auxiliary heating power raised to 100 MW, equivalent operation could be attained with $\eta \sim 0.4$ at a still acceptable fusion gain $Q = 30$, with only a slight increase of impurity seeding compared to the values shown here.

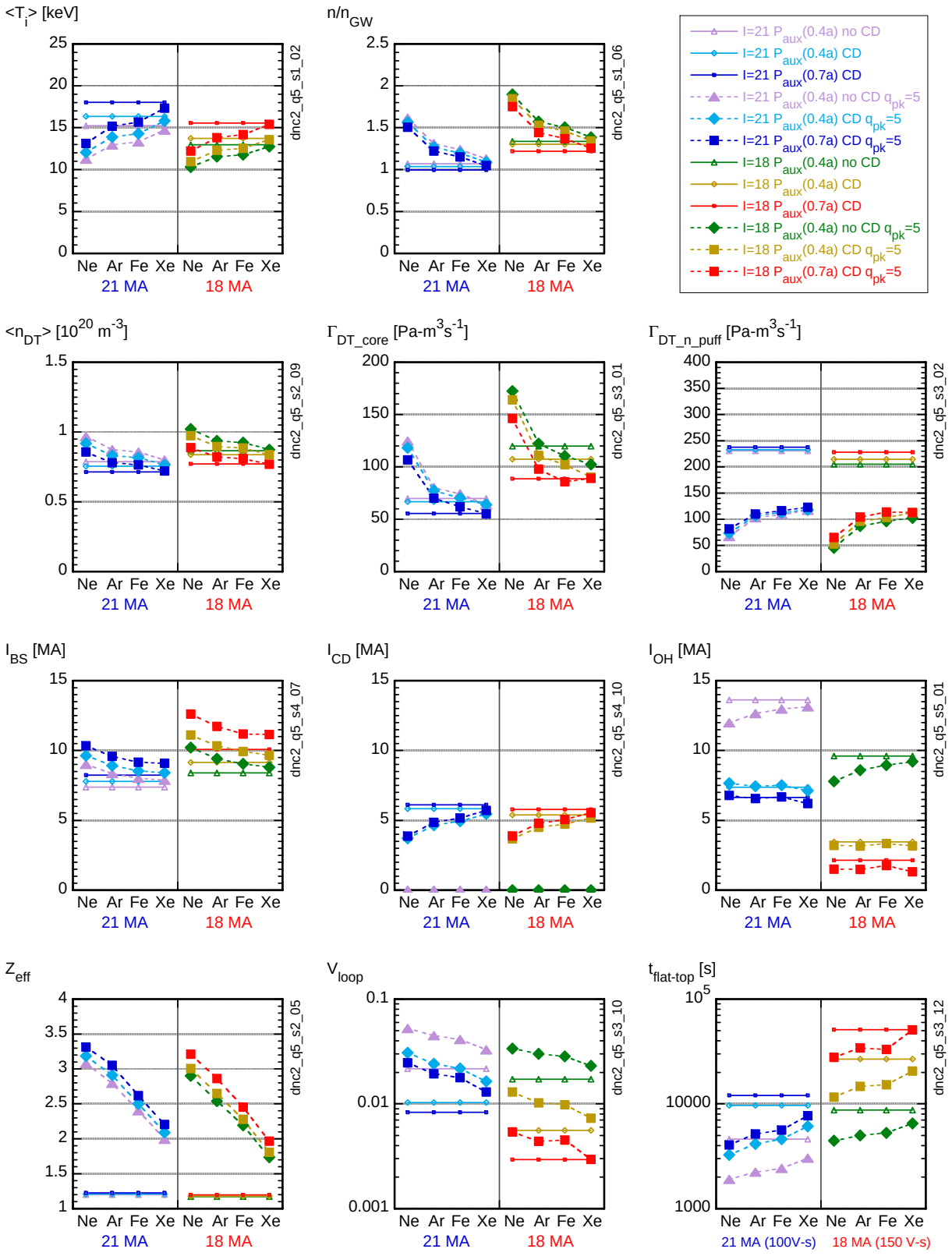

Fig. 5 - Variation of plasma parameters at peak power load q_{pk} of 5 MW/m^2 with seed impurity species at 21 MA (left part of each plot) and 18 MA (right part). Parameters in the absence of impurity seeding are indicated by thin solid lines.

Finally, it should be noted that the ELM-affected zone (the region where the pressure gradient is clamped to the ballooning limit as explained above) is quite large, of the order of 20 cm at

21 MA plasma current, and of 40 cm at 18 MA. The bootstrap current in this region is not negligible, approximately 3.5 MA at 18 MA plasma current. It is likely that there is an increased resistivity associated with the ELMing cycle which would increase the loop voltage necessary to maintain the inductive current. This effect has not yet been evaluated.

6. Conclusions

Integrated core and edge/divertor modelling of prototypical DEMO ELM'y H-mode operation with medium- to high-Z impurity seeding has demonstrated that the peak divertor power load can be reduced to a level compatible with helium-cooled divertor operation, ie. below about 7 MW/m^2 and down to 5 MW/m^2. The core plasma simulation is linked to the SOL and divertor plasma simulation via scaling relationships determined from extensive series of B2-Eirene SOL simulations. The transport model used is that calibrated to JET and Asdex-UG experimental results and previously applied to ITER. Very flat profiles result for electrons and seed impurities.

Several caveats exist in the model. These include notably the validation of impurity transport, the effect of ELM's on overall plasma resistance, and the effect of the seed impurity on the SOL/divertor region. This last effect introduces a new strong coupling between core plasma and divertor operation, which is not presently addressed in the coupled simulation.

Long-pulse operation with scenarios degraded by the impurity seeding required to obtain low peak power loads was investigated for four different seed impurities from Neon to Xenon, at two different plasma currents (21 and 18 MA) with two different profiles of current driven by additional heating (max. near 0.4 and 0.7 of minor radius). The fusion power was held at 3 GW by adjusting the plasma density. An additional heating/current drive power of 50 MW was applied, giving Q=60 operation.

For the same fusion power, the normalized beta increases from 2.6 to a moderately optimistic value of 3.1. Whereas the ratio of density to Greenwald limit increases from 1.1 to 1.3, the density remains at 0.7 of the edge-based density limit. Effective long pulse operation is obtained. With a moderate decrease of plasma current and employing current drive to maximize the bootstrap current. Assuming a reasonable flux available for burn at nominal plasma current (e.g. $\Delta\Phi$(21 MA) ~ 100 Vs), the pulse length would be ~3000s without seeding, and ~4500 s with a peak power load reduced to 5 MW/m^2 by Xenon seeding. The reduction of plasma current leads to an increase in the flux available for burn ($\Delta\Phi$(18 MA) ~ 150 Vs). This, together with off-axis current drive and the resultant increase in bootstrap current, permits a pulse length of ~50,000 s at the same reduced power load.

Future work is intended to examine the effect of ELM's on core plasma resistive losses, to include seed impurities in SOL/divertor modelling, and to investigate the effect of improved confinement as observed in the hybrid operation of present experiments.

References

[1] Pacher, G.W., et al., Plasma Phys. Contr. Fus. **46** (2004) A257
[2] Pacher, G.W., et al., Nucl. Fusion **45** (2005) 581
[3] Kukushkin, A.S., Pacher, H.D., et al., Nucl. Fusion **45** (2005) 608
[4] Pacher, H.D., Kukushkin, A.S., et al, 17th PSI Conf., Hefei (2006), subm. to J. Nuc. Mat.
[5] Bateman, G., Kritz, A.H., et al., Phys. Plasmas **5** (1998) 1793
[6] http://w3.pppl.gov/NTCC/MMM95/
[7] G. Janeschitz, G.W.Pacher, H.D. Pacher et al., 33rd EPS Conf. on Plasma Physics (2006)
[8] Houlberg, W.A., from w3.pppl.gov/rib/repositories/NTCC